CHINESE JOURNAL OF PHYSICS VOL. 38, NO. 1 FEBRUARY 2000

Broken Symmetries in the One-Dimensional Extended Hubbard Model

H. Q. Lin[1], D. K. Campbell[2], and R. T. Clay[2]
[1]*Department of Physics, Chinese University of Hong Kong, Shatin, N. T., Hong Kong*
[2]*Department of Physics, Univ. of Illinois at Urbana-Champaign, 1110 West Green Street, Urbana, IL 61801*

(Received September 6, 1999)

We present analytical and numerical studies on the phase diagram of the one-dimensional extended Hubbard model.

PACS. 75.10.–b – General theory and models of magnetic ordering.
PACS. 75.10.Jm – Quantized spin models.

I. Introduction

The past two decades have witnessed the discoveries of several new classes of novel electronic materials. Ranging from conducting polymers through charge transfer solids and inorganic chain compounds to organic and high temperature superconductors, these materials have in common two important, unusual properties. First, their electronic structures are strongly anisotropic, in some cases (*e.g.*, the chain-like conducting polymers) rendering them quasi-one dimensional, and in others (*e.g.*, the planar copper oxide-based high temperature ("high T_c") superconductors) causing them to be quasi-two dimensional. Second, electron-electron Coulomb interactions play a considerably more important role than in normal metals [1].

Accordingly, considerable recent theoretical effort has been directed towards (idealized) models of "strongly correlated electrons in reduced dimensions," the most celebrated example of which is the one-dimensional Hubbard model. In the Hubbard Hamiltonian, the Coulomb interactions are caricatured by a single parameter U representing the repulsion when two electrons occupy the same site. Remarkably, this model is "integrable" [2] in that an exact solution can be obtained by Bethe *Ansatz* techniques [3]. Despite its considerable analytic appeal and historical importance, the one-dimensional Hubbard model is limited in its applicability to the real novel materials, in which there is considerable evidence for the essential role of longer-ranged Coulomb interactions. For instance, the "excitonic" effects observed in conducting polymers such as polydiacetylene (PDA) and poly-paraphenylene-vinylene (PPV) can not be explained $[1, 4]$ without invoking at least a nearest-neighbor Coulomb repulsion, conventionally called V.

Considering simultaneously both an on-site U and a nearest-neighbor V leads to the "extended Hubbard model", which has recently been the subject of intense interest. In its one-dimensional variant, appropriate for modeling conducting polymers, certain charge-transfer solids, and related materials, the extended Hubbard model is described by the Hamiltonian

$$H = -t \sum_{i=1,\sigma=\uparrow\downarrow}^{N} (c_{i\sigma}^{\dagger} c_{i+1\sigma} + h.c) + U \sum_{i=1}^{N} n_{i\uparrow} n_{i\downarrow} + V \sum_{i=1}^{N} n_i n_{i+1} \tag{1}$$

where $n_{i\sigma} = c^{\dagger}_{i\sigma} c_{i\sigma}$ and $n_i = n_{i\uparrow} + n_{i\downarrow}$. In addition to the explicit parameters U and V modeling the Coulomb interaction, this Hamiltonian has an implicit parameter, $\rho = N_e/N$, where N_e is the total number of electrons and N the number of sites. Although band theory applies only in the absence of strong electron correlations, ρ is conventionally called the "band filling."

Given their role as caricatures of the Coulomb interaction, it is natural to expect that in applications to real materials, only positive values of U and V should be considered. In fact, however, there are at least two reasons for studying negative values as well. First, in some materials, other interactions ($e.g.$ electron-phonon or exciton) can renormalize U and V and lead to negative "effective" values. Second, results from the negative U and V regions provide important benchmarks for other calculations, because in this region superconducting fluctuations occur for a wide range of couplings. The value ρ is determined by the material. Conducting polymers, for example, have $\rho = 1$ ("1/2 filled") in their pristine insulating states and $\rho \simeq 1$ in their doped, conducting states [1]. Charge transfer salts can have a range of values of ρ: TTF-TCNQ, for instance, goes from an incommensurate value of $\rho \sim 2/3$ to the commensurate $\rho = 2/3$ as a function of pressure, [5] while the "Bechgaard salts" have $\rho = 1/2$ ("quarter filled") [6].

The Hamiltonian Eq. (1) exhibits various symmetries that allow us to limit the range of parameters we must study. For instance, by a canonical particle-hole transformation, $c_{i\sigma} = (-1)^i c^{\dagger}_{i\sigma}$, one obtains $\tilde{\rho} = 1 - \rho$ and $\tilde{H} = H + (U + 4V)(N - N_e)$, which differs from the original Hamiltonian by a constant irrelevant in the canonical ensemble (fixed ρ). Thus we can restrict ourselves to band fillings less than 1/2. Another transformation, which we will describe in more detail in later sections, takes the positive Hubbard U model to the negative U Hubbard model (and in addition introduces a magnetic field).

In view of its broad potential relevance to real materials, the extended Hubbard model has been studied extensively by a variety of techniques. On the basis of energy level statistics, it is known to be "non-integrable" for general values of the parameters [2] and thus not amenable to exact solution (except at special values such as $V = 0$). The classic "g-ology" investigations [7, 8] and more recent renormalization group [9] and bosonization [10] studies have provided analytic insight, particularly in the weak coupling regime. Both exact diagonalization calculations [11] and quantum Monte Carlo simulations [12-15] have clarified a number of questions at intermediate and strong coupling [16].

However, most of these calculations have focused on the half-filled case, with the central issue being the location of spin-density wave (SDW)/charge-density wave (CDW) boundary line, as well as the existence and location of a tricritical point [12-15, 17]. Recently, several works have examined the the quarter-filled case ($\rho = 1/2$) and suggested the possibility of superconductivity in an unexpected region of the U, V parameter plane [18, 19]. However, systematic studies of the phase diagram of the one-dimensional extended Hubbard model as a function of all three parameters (U, V, ρ) have not been carried out although there exist some work for specific band fillings [20]. The purpose of this article is to give a rather detailed review on our recent studies of the one-dimensional extended Hubbard model. Both analytically and numerically, we study the phase diagram throughout the full parameter space, determine the nature of the different phases, and describe the quantitative behavior of the spin-spin, charge-charge, and superconducting pairing correlation functions and related susceptibilities. In particular, we will identify the values of the parameters for which the extended Hubbard model behaves as a "Luttinger liquid" [21] and exhibits the conductivity properties of a highly correlated metal.

The remaining sections of the article are organized as follows. In Sections II and III, we present an overview of the concepts and methods we use, discussing broken symmetries in the strong-coupling limit, reviewing weak-coupling results abd properties of a Luttinger liquid, describing our quantum Monte Carlo and exact diagonalization algorithms. Section IV contains our quantitative calculations, both analytic and numerical, of the phase diagram; for clarity, the results are organized by parameter region, rather than by technique. This section provides the essential calculational details supporting results announced in Ref. [22]. We conclude in Section V, with a summary and discussion of open problems, both theoretical and related to comparisons with real materials.

II. Broken symmetry states

II-1. Strong coupling limit

Although most previous studies of the extended Hubbard model have focused on the weak-coupling limit, we shall later see that perturbation theories based on the strong-coupling limit provide considerable semi-*quantitative* insight into the various phases of this model. Further, elementary strong coupling considerations provide insight into nearly all the broken symmetry phases we shall encounter. Accordingly, we shall begin our discussion with some qualitative remarks on broken symmetries in the strong coupling regime. Since we are ignoring electron-phonon interactions, the competing phases are limited to charge-density-waves (CDW), spin-density-waves (SDW), superconductivity (SC), and phase separation (PS). In the limit of very strong Coulomb interactions, i.e., $|U|, |V| \gg t$, one can easily characterize the CDW, SDW, and PS states in "real" space. This limit formally coincides with the $t = 0$ limit, which is sometimes called the "classical" (because the quantum effects due to hopping vanish) or "atomic" (because the individual sites are isolated) limit.

In a CDW state, the electron density is not uniform but has a periodic modulation. One CDW eigenstate of the extended Hubbard model with $t = 0$ in the half-filled case ($\rho = 1$) has the form shown in Fig. 1(a). Clearly, whether this state will be the ground state depends on the values of U and V: for instance, for both U and V positive and $U < 2V$, one can show that this CDW is indeed the ground state at half-filling.

Similarly, in an SDW state, the spin density that varies from site to site, leading to an algebraic (antiferro-)magnetic ordering. For instance, for quarter filling ($\rho = 1/2$), one $t = 0$ SDW eigenstate has the form shown in Fig. 1(b). In the standard parlance (which is based on weak coupling), this state would correspond to a "$2k_F$ SDW" and a "$4k_F$ CDW", since for lattice spacing a the relationship between $\rho = 1/2$ and k_F is $k_F a \equiv \pi\rho/2$, so that a $2k_F$ variation has period 4 and a $4k_F$ variation period 2.

In a phase separated state, the ground state becomes macroscopically inhomogeneous, with different spatial regions having different average charge densities. In Hubbard-like models, phase separation is usually driven by the absence of long-range Coulomb interactions and *typically* occurs for *attractive* ($i.e.$, negative) values of U and V, so that the electrons cluster together in order to gain as much negative potential energy as possible. In the extended Hubbard model, one can readily identify two types of phase separated configurations, which we shall call PS_1 and PS_2. In a static PS_1 state, electrons form a cluster of singly occupied sites, as shown in Fig. 1(c), while in a static PS_2 state, electrons form a cluster of doubly occupied sites, as in Fig. 1(d). Obviously, the PS_2 state would be favored for negative U and negative V, whereas the the PS_1 state would

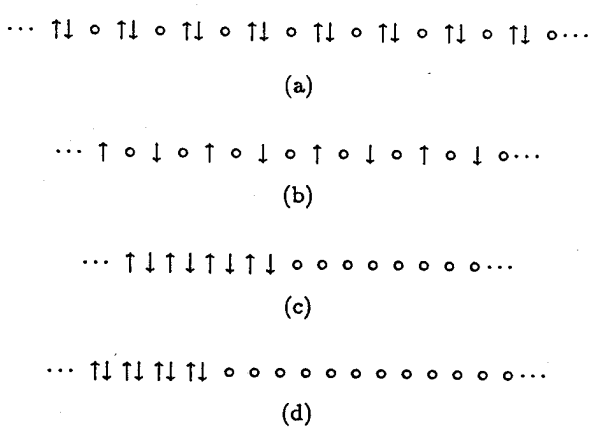

FIG. 1. Real space configurations corresponding to certain broken symmetry phases in the "strong coupling" ($t = 0$) limit; (a) a "$2k_F$" CDW state for $\rho = 1$; (b) a co-existing "$2k_F$ SDW" and "$4k_F$ CDW" state at $\rho = 1/2$; (c) a PS_1 phase separated state; and (d) a PS_2 phase separated state.

be favored for positive U and negative V.

When the hopping t is included, the simple real space configurations corresponding to the strong coupling "cartoons" in Fig. 1 are no longer eigenstates of the Hamiltonian, and we must undertake detailed calculations to study the competition among possible broken symmetries. These will be discussed in the next section.

II-2. Weak coupling limit

Since the results in this regime are well known and nicely summarized in Ref. 7, we will recall briefly only a few key points, saving more detailed comments for later comparisons with strong coupling and numerical results. In the limit of weak coupling ($|V|/t, |U|/t \gg 1$), the non-interacting hopping term dominates, and for low energies the physics is governed by properties near the Fermi surface, which for 1D consists of only 2 points, i.e., $\pm k_f$ ("left-going" and "right-going" particles). In this regime the bandwidth can be taken (formally) to infinity. This amounts to take a continuum limit in which the momentum dependence of the Hamiltonian linearized. The resulting theory is mapped into an effective theory of relativistic fermions, the Luttinger model and its corrections. Interested readers can find the one-to-one correspondence between coupling constants in this "g-ology" picture and the extended Hubbard model in Table I of reference 7.

An alternative, and more general approach to this problem, is offered by bosonization [10, 21, 23-25] In the bosonized Hamiltonian, the charge degrees of freedom separate from the spin degrees of freedom, if one ignores terms that are irrelevant in the renormalization group sense. The backward scattering affects only the spin-density waves and the umklapp scattering (in which electrons of opposite spin cross the Fermi surface in the same direction) affects only the charge-density waves, so that these two kinds of collective mode do not mix.

By determining which of the various correlation functions dominates in a given region of parameter space, the "g-ology" or bosonization approaches can construct a phase diagram, which

predicts CDW, SDW, and both singlet and triplet superconducting phases. Although bosonization schemes can be developed to include higher order commensurability effects, in the simplest "g-ology" approach the half-filled band is singled out as the only band filling for which umklapp effects are significant. All other band fillings – including the case of quarter-filling, which as we shall see is of particular interest for the extended Hubbard model – are effectively "incommensurate." In this respect, as well as in the absence of any indication of phase separation, the (lowest-order) weak coupling, continuum results differ from the full lattice calculations we describe in the sequel.

III. Numerical approaches

While in both strong and weak coupling limits one can perform quite well analytical analysis on various broken symmetry phases, numerical approaches are called for when the hopping amplitude is comparable to Coulomb interactions, the so called intermediate coupling case. Two well developed numerical techniques were used in our studies: the quantum Monte Carlo simulation and the exact diagonalization of the Hamiltonian.

III-1. Quantum monte carlo simulations: correlation functions and susceptibilities

In weak coupling theories, the phase diagram of interacting electrons is studied by determining the character of the dominant fluctuations in a given region of parameter space. To generalize this approach for arbitrary coupling, we need to study the behavior of correlation functions and susceptibilities as functions of the parameters and the system size. To measure these quantities, we use the world-line quantum Monte Carlo, as described in Ref. 26, and thus work in the canonical ensemble. We investigate the behavior of the charge-charge and spin-spin correlations as we increase the lattice size and lower the temperature. Explicitly, we calculate the Fourier transform of charge-charge correlation:

$$C(q) = \frac{1}{N\beta}\int_0^\beta d\tau \sum_{i,j}^{N} \langle (n_{i\uparrow}(\tau) + n_{i\downarrow}(\tau))(n_{j\uparrow}(\tau) + n_{j\downarrow}(\tau))\rangle e^{iq(i-j)} \tag{2}$$

where

$$q = \frac{2\pi}{N}(0, 1, ..., N-1). \tag{3}$$

In the perfect CDW state for $\rho = 1/2$ as shown in Fig. 1(a), $C(q = 4k_F = \pi)$ diverges as N increases, whereas in the phase separated states (both PS_1 (Fig. 1(c)) and PS_2 (Fig. 1(d)), $C(q = \frac{2\pi}{N})$ diverges. In addition to the charge correlations, we study also the zero-frequency CDW susceptibility, defined by:

$$\chi_{CDW}(q) = \frac{1}{N\beta}\int_0^\beta d\tau \sum_{i,j}^{N} \langle (n_{i\uparrow}(\tau) + n_{i\downarrow}(\tau))(n_{j\uparrow}(0) + n_{j\downarrow}(0))\rangle e^{iq(i-j)} \tag{4}$$

To study the SDW phases, we examine the spin-spin correlation function and the zero-

frequency SDW susceptibility, respectively defined as:

$$S(q) = \frac{1}{N\beta}\int_0^\beta d\tau \sum_{i,j}^{N}\langle(n_{i\uparrow}(\tau) - n_{i\downarrow}(\tau))(n_{j\uparrow}(\tau) - n_{j\downarrow}(\tau))\rangle e^{iq(i-j)} \tag{5}$$

and

$$\chi_{SDW}(q) = \frac{1}{N\beta}\int_0^\beta d\tau \sum_{i,j}^{N}(n_{i\uparrow}(\tau) - n_{i\downarrow}(\tau))(n_{j\uparrow}(0) - n_{j\downarrow}(0)) > e^{iq(i-j)} \tag{6}$$

We expect, for instance, that for $\rho = 1$, $\chi_{SDW}(q = \pi)$ should diverge in the SDW phase but be very small in both the CDW phase and the phase separation regions.

To distinguish the two distinct phase separated phases (PS_1 and PS_2) we cannot simply use the criterion that $C(q = \frac{2\pi}{N})$ diverges, because it does so in both phases. Hence, we use a histogram of site occupation numbers [14]. Since the total number of particles is fixed in the canonical ensemble, we measure particle occupations in a certain "window", $i.e.$, a certain number of adjacent sites. For a uniformly distributed charge density, the histogram will have a peak at $n = \rho$. For the PS_1 state, it will have peaks around $n = 0$ and 1. For the PS_2 state, it will have peaks around $n = 0$ and 2; we will present the results in our later discussion.

Most of our QMC simulations were carried out on lattices of up to 64 sites and at temperatures down to $T = 0.0625$ in the units $t = 1$, and we have checked in several cases using longer chains and lower temperatures that our results are in the thermodynamical limit within QMC statistical errors.

III-2. Exact diagonalization studies: luttinger liquid parameters and superconducting order parameters

Our exact diagonalization calculations used a Lanczös algorithm [27]. We obtain the ground state energy and eigenvector and then calculate the critical exponent, K_ρ, based on the Luttinger liquid theory. The term "Luttinger liquid" was coined by Haldane [21], based on the properties of the Tomonaga-Luttinger model [28], to describe certain one-dimensional models of interacting electrons whose properties differ sharply from ordinary Fermi liquids. As discussed by several authors [21, 28-32], the characteristics of a Luttinger liquid include: (1) the vanishing of the quasi-particle residue at Fermi surface, $Z_F = 0$, reflecting the absence of a discontinuity at the Fermi surface and its replacement by a power-law behavior $(k-k_F)^\alpha$, indicating a collective rather than a quasi-particle-like behavior, with α related to the asymptotic power-law decay of the Green's function at large distance, and dependent in detail on the interaction strength; (2) the existence of gapless, collective excitations which, in the continuum limit, are describable by conformal field theories with independent velocities for each of the gapless modes; and (3) the ability to express all the correlation functions of the model in terms of a single exponent, K_ρ. The charge-charge and spin-spin correlation functions at long distance have power divergence with leading exponents $\mu_{CDW} = \mu_{SDW} = -1 - K_\rho$, while the singlet and triplet superconducting pairing function have $\mu_{SS} = \mu_{TT} = -1 - 1/K_\rho$. Thus if $K_\rho > 1$, the superconducting fluctuations dominate whereas if $K_\rho < 1$, the CDW and SDW fluctuations dominate. Since for a Luttinger liquid the dominant fluctuations are determined exclusively by K_ρ, we can determine the boundaries of the Luttinger liquid regions (and hence most of the phase diagram) by plotting the contours of constant K_ρ.

Moreover, Luttinger liquid theory also relates bulk quantities, such as the compressibility κ and the Drude weight D_c, to K_ρ [32]. Specifically, the following relations among the central charge c, the compressibility κ, the charge velocity v_c, the spin velocity v_s, and the Drude weight D_c, were established for Luttinger liquids [30-32]: (i) $E(N) = E_\infty - \frac{1}{N^2}\frac{\pi c}{6}(v_c + v_s)$, (ii) $K_\rho = \frac{\pi}{2}\rho^2\kappa v_c$, (iii) $D_c = \frac{1}{\pi}K_\rho v_c$, where N is the system size. To evaluate the discrete compressibility we use

$$\kappa^{-1} = N_e^2 \frac{e(N_e+1) + e(N_e-1) - 2e(N_e)}{4} \tag{7}$$

where $e(N_e)$ is the ground state energy per site at density $\rho = N_e/N$. A diverging κ implies that phase separation has occurred, and this can be used as a check of the Monte Carlo results for this boundary line. To obtain the Drude weight, we calculate the finite-size corrections to the ground state energy with twist on the boundary conditions [33, 34]. The charge and spin velocities were obtained from the lowest frequency pole ω_l of the charge-charge and spin-spin response functions [35] by, $v_l = \frac{\omega_l(k_1)}{k_1}$, where $k_1 = \frac{2\pi}{N}$ and l refers to spin or charge. Therefore, we determine directly both velocities without following adiabatically the relevant low-energy excitations. The central charge was then obtained by fitting $E(N)$ and using the conformal field theory prediction for finite-size corrections to the ground state energy. For results presented in this article, we performed exact diagonalization calculations on lattices of up to 16 sites. The boundary conditions were imposed so that there is no degeneracy at Fermi surface for the non-interacting case and that there will be no net current flow in the ground state.

In order to distinguish among different possible superconducting states, we have also calculated various superconducting correlation functions in our exact diagonalization studies. The superconducting pairing correlation is defined by:

$$P_{lm} = \langle \Delta_l^\dagger \Delta_m \rangle \tag{8}$$

Here Δ_l is a pairing operator:

$$\Delta_l = \frac{1}{\sqrt{N}} \sum_i c_{i+l\uparrow} c_{i\downarrow}, \tag{9}$$

where l is a displacement vector on the lattice. Pair operators of various symmetries can be constructed from linear combination of Δ_l's, including nearest-neighbor singlet ($\Delta_s = \Delta_x + \Delta_{-x}$), nearest-neighbor triplet ($\Delta_t = \Delta_x - \Delta_{-x}$), and on-site singlet ($\Delta_0$) operators. As we discuss below, the behaviors of these pairing correlations as functions of band filling and Coulomb interactions U and V reveal different dominant symmetry in the superconducting state in different regions of parameter space.

IV. Phase diagram

IV-1. Overview of the phase diagram

In Figs. 2, 3, and 4 we provide an overview of the phase diagram of the extended Hubbard model as a function of its three parameters U, V, and ρ. Figure 2, which is redrawn from Ref. [14], reproduces the well-known results for the half-filled case [7, 11, 12, 14]. Fig. 3 illustrates

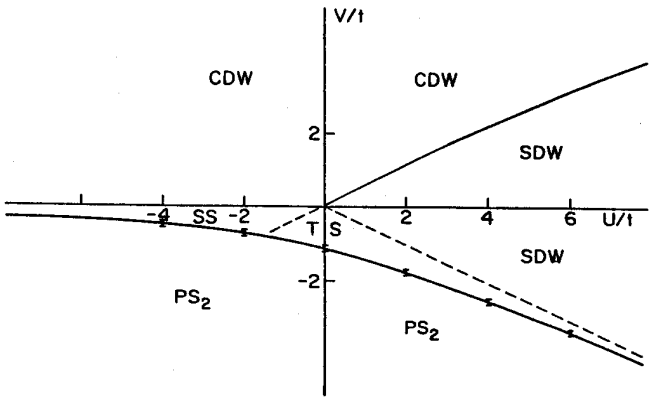

FIG. 2. The phase diagram of one-dimensional extended Hubbard model at $\rho = 1$. The dashed lines are $U = -2V$ and $U = 2V$, respectively. The thickness of the line separating the CDW/SDW regions indicates the nature of the phase transition: the thin line at weaker coupling is a second-order transition, whereas the thicker line for stronger coupling is a first-order transition. The symbols are the QMC results with statistical errors. The "g-ology" results are fully consistent with this figure in the weak coupling region (This figure is redrawn after Ref. [14]).

our results for the particularly interesting case $\rho = 1/2$, about which several studies have recently appeared [18, 19] to complement the early studies [13] of this case. Finally, in Fig. 4 we show the phase diagram as a function of band filling and V for a representative values of U.

In the following subsections, we present in detail the calculations which support these figures. Our calculations include (1) perturbation theory analyses in various strong coupling limits, where the kinetic part of the Hamiltonian is treated perturbatively and in the weak coupling limit, where the kinetic energy dominates; (2) analytic calculations of a two-body problem to determine the phase boundary between superconducting phase and PS_1 phase; (3) quantum Monte Carlo results to determine phase boundaries in the intermediate coupling region U, $V \sim 4t$; and (4) exact diagonalization calculations to find the contours of constant K_ρ and the transition line where $K_\rho = 1$ (and hence to determine the location of a superconducting phase) numerically on finite lattices.

The limited number of finite lattices that can be studied in detail (N=4, 6, 8, 10, 12, and 16 for some of band fillings) does not in general permit us to do proper finite-size scaling. Worse still, for a given band filling, the problems of requiring different boundary conditions for $N_e = 4n$ and $N_e = 4n + 2$ and the need to preserve up-down spin symmetry in fact mean that we often have only two or three lattices available for a given band filling for calculating K_ρ. Nonetheless, our data do seem to indicate good agreement (5-10% errors) with the infinite system results. For instance, for $U = 8$, $V = 0$, and $\rho = 0.50$, we find for $N = 4, K_\rho \simeq 2.24$ and for $N = 8$, $K_\rho \simeq 2.44$, while in the thermodynamic limit, $K_\rho \simeq 2.49$.

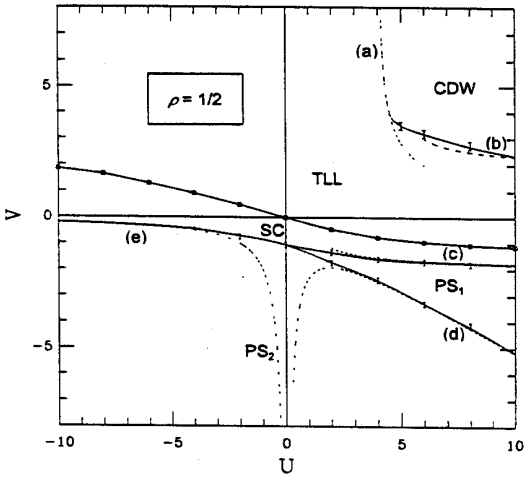

FIG. 3. The confirmed features of the phase diagram of the one-dimensional extended Hubbard model for quarter filling ($\rho = 1/2$). The symbols are our QMC results with statistical errors through which solid curves have been fitted to guide the eye. The dotted/dashed lines labeled (a) to (e) are various second-order, strong-coupling perturbation theory results (see the text for details).

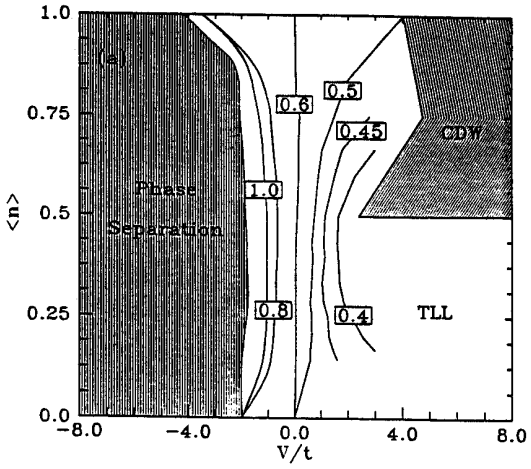

FIG. 4. Contours of K_ρ on the $\rho - V$ plane for $U = 8t$. Regions of phase separation and the "CDW/HLL" region are also shown (see text). Superconductivity exists in the regions between the $K_\rho = 1.00$ contours and the phase separation regions.

Although weak coupling perturbation theory is perhaps more familiar and more commonly used, our studies have shown that for the 1-D extended Hubbard model the strong coupling limit provides much greater insight into the general behavior of the model in all parameter regimes, including effects of changes in band filling. As we shall see, these analytical studies provide an appealing and convincing framework for the phase diagram of the extended Hubbard model. Basically, the results of $|U|, |V| > 4t$ fall in the strong coupling regime, and the Monte Carlo results are almost indistinguishable from second-order perturbation theory calculations, whereas those for $|U|$, $|V| < 4t$ fall in the weak coupling regime. Our results suggest that $U = \infty$, $|V| = \infty$; and $U = V = 0$ are "fixed points" of this model in the RG sense.

To organize our subsequent discussion clearly, we divide it into three major subsections, dealing with (1) $U < 0$; (2) $U > 0$, $V < 0$; and (3) $U > 0$, $V > 0$. Since it is less complex and will allow us to introduce our approach in a relatively simple context, we start with the case of *negative* U.

IV-2. The phase diagram for negative U

For negative U, the attractive on-site interactions cause electrons to tend to occupy the same

site. From a variety of studies of the Hubbard and related models [37] in this regime, we expect that, independent of ρ, superconducting fluctuations will be the dominant homogeneous broken symmetry and will compete with PS_2-type phase separation. To confirm these speculations, we follow the lead of Emery [16], who pointed out that in the large negative U limit, one can obtain an effective Hamiltonian which, to the second order in the hopping t and to first order in V, takes the form of a Heisenberg model. Following Ref. 16, we first make the following canonical transformation:

$$\begin{aligned} c_{i\downarrow}^{\dagger} &= (-1)^i b_{i\downarrow} \quad c_{i\downarrow} = (-1)^i b_{i\downarrow}^{\dagger} \\ c_{i\uparrow}^{\dagger} &= b_{i\uparrow}^{\dagger} \qquad\quad c_{i\uparrow} = b_{i\uparrow} \end{aligned} \tag{10}$$

so that

$$\begin{aligned} n_{i\uparrow} &= b_{i\uparrow}^{\dagger} b_{i\uparrow} = \eta_{i\uparrow} \qquad n_{i\downarrow} = b_{i\downarrow} b_{i\downarrow}^{\dagger} = 1 - \eta_{i\downarrow} \\ S_i^{\dagger} &= b_{i\uparrow}^{\dagger} b_{i\downarrow} = (-1)^i c_{i\downarrow}^{\dagger} c_{i\uparrow}^{\dagger} \qquad S_i^{-} = b_{i\downarrow}^{\dagger} b_{i\uparrow} = (-1)^i c_{i\uparrow} c_{i\downarrow} \\ S_{i,z} &= \frac{1}{2}(\eta_{i\uparrow} - \eta_{i\downarrow}) = \frac{1}{2}(n_{i\uparrow} + n_{i\downarrow} - 1) \end{aligned} \tag{11}$$

The extended Hubbard Hamiltonian is transformed into:

$$\begin{aligned} H = & -t \sum_{i=1,\sigma=\uparrow\downarrow}^{N} (b_{i\sigma}^{\dagger} b_{i+1\sigma} + h.c) + |U| \sum_{i=1}^{N} \eta_{i\uparrow}\eta_{i\downarrow} \\ & + 4V \sum_{i=1}^{N} S_{i,z} S_{i+1,z} + (4V - \frac{|U|}{2}) \sum_{i=1}^{N} S_{i,z} - \frac{|U|}{2} \sum_{i=1}^{N} (\eta_{i\uparrow} + \eta_{i\downarrow}) + NV \end{aligned} \tag{12}$$

The average number of pseudoparticles $\langle \eta \rangle = \frac{1}{N}\sum_{i=1}^{N}(\eta_{i\uparrow} + \eta_{i\downarrow}) = \frac{1}{N}\sum_{i=1}^{N}(n_{i\uparrow} - n_{i\downarrow} + 1) = 1$, *provided* we consider the spin-symmetric case ($n_{i\uparrow} = n_{i\downarrow}$ in the original problem); thus in terms of the pseudoparticles we always have a "half-filled" case here. Hence, in the strong coupling limit $|U| \gg t$, this model can be mapped into the XXZ Hamiltonian *in a magnetic field*:

$$\begin{aligned} H_{eff} = & \sum_{i=1}^{N} -(J_x S_{i,x} S_{i+1,x} + J_y S_{i,y} S_{i+1,y} + J_z S_{i,z} S_{i+1,z}) \\ & + \left(4V - \frac{|U|}{2}\right) \sum_{i=1}^{N} S_{i,z} + N\left(V - \frac{|U|}{2} - \frac{t^2}{|U|}\right) \end{aligned} \tag{13}$$

with

$$J_x = J_y = \frac{4t^2}{|U|} \qquad J_z = -J_x - 4V. \tag{14}$$

After this canonical transformation, the order parameters in the original extended Hubbard model can be expressed in the language of the XXZ model. Antiferromagnetic long-range order in the z-direction means that there exists a non-zero value of m such that, $\langle S_{i,z} \rangle = (-1)^i m$. In terms

of the original electron operators, this corresponds to $\langle n_i \rangle = 1 + (-1)^i 2m$, *i.e.*, to a CDW state. Similarly, ferromagnetic long-range order in the z-direction means $\langle S_{i,z} \rangle = m$, which leads to $\langle n_i \rangle = 1 + 2m$ and one gets phase separation. A superconducting state would have non-zero $\langle \Delta \rangle$ and this leads to non-zero $\langle S_i^- \rangle$, *i.e.*, long range antiferromagnetic order in the $x - y$ plane.

Studying Eqs. 12 and 13, we see that the original band filling parameter ρ introduces magnetic field effects in the spin model: $\sum_{i=1}^{N} S_{i,z}$ in Eq. 13 is just $\frac{1}{2}N(\rho - 1)$. Hence for the half-filled band there is no magnetic field, and the phase boundary between the CDW and superconductivity occurs at $V = 0$, since here $J_z = -J_x$. This is shown in Fig. 2. As the band filling decreases from 1, the increasing effective magnetic field will destroy the AFM order in z-direction (and hence the superconductivity in the original model) *unless* the coupling J_z is large enough to compensate for it. That means the phase boundary of superconductivity will move into the $V > 0$ region as $\rho < 1$, which is confirmed by our numerical calculations, as shown in Fig. 5.

When $J_z = J_x$ there is a first-order transition to a ferromagnetic state. In the Heisenberg model, this corresponds to half of the system having spin up and half spin down, since the total magnetization is conserved. In the extended Hubbard model, this corresponds to phase separation, which is of the type PS_2 since $U < 0$. Hence, the transition line in this limit is given by:

$$V_{PS} = -\frac{2t^2}{|U|}. \tag{15}$$

Since a uniform magnetic field has little influence on the ferromagnetic state, the phase boundary in the original electron variables should have little to do with band filling. The QMC results for this phase boundary, which are exemplified by those shown in the lower left quadrant of Fig. 3, are, for $|U| > 4t$, almost identical to these second-order strong coupling perturbation theory results (shown in Fig. 3 as the dashed line labeled (e)).

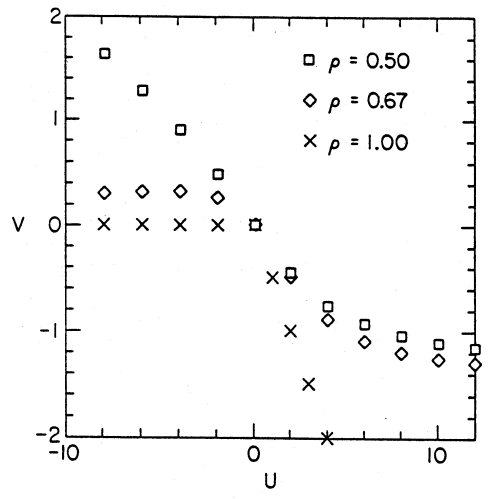

FIG. 5. The "top" boundary of the superconducting phase in the $U - V$ plane for several values of ρ. As discussed in the text, for $\rho < 1$, the superconducting phase can occur over a wider range of values of V.

Finally, we note that for the negative U case, the critical behavior is determined by the gapless excitation spectra of *bound pairs*. The conformal field theory predictions (Eq. 2-4), which are valid for $U > 0$, can also be applied for *negative* U, by taking $v_s = 0$ and v_c as the group velocity of a bound pair at the Fermi surface. For this case, we find $C \sim 1$ at fixed $U = -8t$ and $0 < V < 6t$. The charge-charge correlation exponent at $V = 0$ agrees with the Bethe *Ansatz* results, $K_\rho = 1$ at $\rho = 1$ and $K_\rho \sim 2(1 + \rho/2\sqrt{1 + U^2/16})^{-1}$ at small densities. Note that $K_\rho \to 2$ as $\rho \to 0$. Our numerical results show that this is also true at finite V.

IV-3. $U > 0$**,** $V < 0$

1.Strong coupling calculations

Again we begin with the strong coupling limit and note that for $t = 0$ the extended Hubbard Hamiltonian can be written as

$$H = \sum_{i=1}^{N} H(i) \tag{16}$$

where

$$\begin{aligned} H(i) &= U n_{i\uparrow} n_{i\downarrow} + V n_i n_{i+1} \\ &= \left(\frac{U}{2} + 2V\right) n_i - \left(\frac{U}{2} + V\right) (n_{i\uparrow} - n_{i\downarrow})^2 - \frac{V}{2}(n_i - n_{i+1})^2. \end{aligned} \tag{17}$$

In this limit, n_i commutes with H, so the real-space configurations are eigenstates. In the present case of negative V, an attraction between electrons on neighboring sites, and hence the electrons will cluster together. For arbitrary band filling this leads to the existence of electron-rich and electron-deficient regions of the 1-D system, $i.e.$, to phase separation. Importantly, as discussed above, we can identify the two distinct types of phase separated states, PS_1 and PS_2, whose properties we now study in somewhat more detail in preparation for later applications of the results.

When $V < -U/2$, the system achieves the lowest energy by maximizing the number of double occupancies, so $n_{i\uparrow} = n_{i\downarrow}$ and $n_{i+1} = n_i$, where $N_e/2$ sites are occupied while the rest are empty. The total energy of this PS_2 phase is

$$E = \frac{U}{2} N_e + 2V N_e - 4V \tag{18}$$

where $N_e = \rho N$ is the total number of electrons. For simplicity in Eq. 18 and for the remainder of the text we assume that there are the same number of up spin electrons as down spin electrons; other cases, which are of particular interest when magnetic field effects are included, can be dealt with in a similar manner.

In contrast, when $0 > V > -U/2$, the ground state is the PS_1 phase with N_e singly-occupied sites clustered together and energy

$$E = N_e V. \tag{19}$$

Clearly, for $t = 0$ the transition between the two types of phase separated systems occurs (in the thermodynamic limit) at $U = -2V$, independent of band-filling ρ.

For $t \neq 0$ we use second-order strong-coupling perturbation theory to calculate the corrections to the energies of both states. For the state PS_2, the second-order correction to the ground state energy comes only from the "surface" between the two phases; hence it is of $O(1)$ rather than $O(N)$ or $O(N_e)$ and is irrelevant in the thermodynamic limit, so that the energy of PS_2 is still given by Eq. 18. In contrast, in the state PS_1 the correction arises throughout the volume and hence is of order $N_e = \rho N \sim N$. Using standard techniques [38], we obtain an effective Hamiltonian on the occupied sites

$$H = V \sum_i n_i n_{i+1} + J \sum_i (S_i S_{i+1} - 1/4 n_i n_{i+1}), \tag{20}$$

with $J = 4t^2/(U - V)$. Hence the ground state energy (using the Bethe *Ansatz* result [39]) is

$$E = N_e \left(V - \frac{4t^2 \ln 2}{U - V} \right), \tag{21}$$

where $N_e = \rho N$.

Equating the energies of the PS_1 and PS_2 states, we can determine the phase boundary between them in the strong coupling limit as $N \to \infty$ in the region $U > 0$, $V < 0$:

$$V = -\frac{U}{2} - \frac{8t^2 \ln 2}{3U}. \tag{22}$$

Thus, to this order in perturbation theory, *there is no band-filling dependence for this phase boundary*. Finite-size effects and higher order corrections will change this result, but as we shall see later it provides a remarkably accurate guide to our numerical results. This boundary is plotted in Fig. 3 as the dashed line labeled (d).

For $t \neq 0$, the attraction represented by negative V can lead not only to phase separation but also to superconductivity. Based on recent studies in related models [40], as well as earlier work on the extended Hubbard model [12-14], we expect superconductivity to occur near the phase separation boundary but at slightly less attractive values of V. We determine the superconducting (SC) phase boundary numerically by calculating K_ρ on finite lattices using the Lanczös techniques described above. This phase boundary is plotted in Fig. 3 for the 1/4-filled case. For other band fillings, our calculations show that, as $\rho \to 1$, the phase boundary moves down towards the $U = -2V$ line for $U > 0$ (sandwiched by SDW and PS_1 phases), and towards the $V = 0$ line for $U < 0$ (sandwiched by CDW and PS_2 phases).

To distinguish this superconductivity from phase separation, we can again use perturbation theory to estimate the phase boundary. For $U \to \infty$, we can readily show that the phase boundary is $V_c = -2t$, since as our earlier manipulations on XXZ model show, for $V < -2t$, the ground state has ferromagnetic long-range order, which corresponds to phase separation in the extended Hubbard model. When U is finite, the total energy in the phase separated PS_1 region is:

$$E_{PS} = (N_e - 1) \left(V - \frac{4t^2 \ln 2}{U - V} \right). \tag{23}$$

To study the superconducting phase, which consists of paired electrons, we focs on the regime in which two particles form a bound state and hence have lower energy than two separate, free particles. Thus we consider removing two electrons from the PS_1 state and calculating the total energy, E_{BS}, of the two-particle bound state, which is determined by

$$2V\left(1-\frac{E_{BS}}{U}\right)=(E_{BS}-\sqrt{E_{BS}^2-16t^2})\left(1+\frac{1}{U}\sqrt{E_{BS}^2-16t^2}\right). \tag{24}$$

At the SC/PS phase boundary, we also have

$$E=2\left(V-\frac{4t^2\ln 2}{U-V}\right). \tag{25}$$

We obtain the SC/PS phase boundary by solving Eqs. 24 and 25 numerically; the resulting boundary is depicted in Fig. 3 (the line labeled (c)).

From recent studies of phase separation in related models [40], we also expect the possibility of forming three, four, or more particle bound states near the SC/PS phase boundary. We have investigated these multi-particle bound states by performing exact diagonalization calculations on finite lattices and using finite-size scaling. The results show that the region between superconducting state and phase separation, *i.e.*, the region in which there exist multi-particle bound states, is very small. For example, at $U=4t$, we find a dilute gas of paired electrons for $-1.61t<V<-t$, a four-particle bound state beginning at $V\simeq -1.61t$, and phase separation at $V\simeq -1.7t$; hence the multi-particle bound states only occur in the small region $-1.7t<V<-1.61t$. This region becomes still smaller as U increases, and we have chosen not to plot it in Fig. 3.

2. Weak Coupling: The limiting case $U=0$

Since several of our strong coupling results diverge as $U\rightarrow 0$, we should show that it is also possible to gain analytic insight into this weak coupling limit by considering explicitly the case of $U=0$. We start from the strongly phase separated region, with $|V|\gg t$. For $U=0$, this region will have all sites doubly occupied (*i.e.*, it will be the PS_2 state. Removing one electron from this region leads to a gain of kinetic energy (-2t) and a loss of potential energy (2V), so the instability to phase separation seems to occur at $V=-t$. However, the attractive interaction can lead to a two-body bound state. Indeed, the critical value of V for forming a bound state is $V_{2c}=-2t/(1+4t/U)$, which is 0 for $U=0$ so the instability to the formation of pairs occurs immediately for $V<0$.

To find a more precise estimate, as a function of ρ, of the value of V_{PS} at which phase separation occurs for $U=0$, we adopt a mean-field variational argument, the motivation for which comes from the known applicability of mean field theory to weak-coupling superconductivity and the validity of which will be establish *post hoc* by agreement with our numerical results. Using the wave function of the free electron gas as a trial state, we find the expectation value of H to be

$$E_{var}=\langle H\rangle_{free\ electron\ gas}=-N\left[\frac{4t}{\pi}\sin(k_F)+V\rho^2-\frac{2V}{\pi^2}|\sin(k_F)|^2\right] \tag{26}$$

where $k_F=\frac{\pi}{2}\rho$ is the Fermi momentum. The energy for the PS_2 state is

$$E_{PS}=2VN_e-4V \tag{27}$$

Equating these two energies, we find the critical value of V_{PS} as a function of ρ to be

$$V_{PS} = -\frac{\frac{4t}{\pi}\sin(k_F)}{2\rho - \rho^2 + \frac{2}{\pi^2}|\sin(k_F)|^2} \tag{28}$$

which is $-1.05870t$ for $\rho = 1$ and $-1.05755t$ for $\rho = 1/2$. Our QMC numerical calculations give critical values $V_{PS}/t = -1.15 \pm 0.05$ and -1.05 ± 0.05, respectively. We note that the $-4V$ term in Eq. 27, which vanishes in the thermodynamic limit, nonetheless contributes to finite-size effects in Monte Carlo simulations and exact diagonalization calculations. Such effects can be substantial for small lattices such as $N = 12$.

Once again, our analysis shows little dependence on band filling. In fact, from this variational calculation, the critical values of V are bounded between $-1.05938t$ (for $\rho = 0.69$) and $-t$ (for $\rho = 0$). Based on these estimates, we expect that the transition to phase separation to be around $V = -t$ for all band fillings, consistent with our numerical simulations.

If we turn on the interaction U and perform a similar calculation, we obtain the phase boundary to be

$$V = -\frac{\frac{4t}{\pi}\sin(k_F) + U(\frac{1}{2} - \frac{\rho}{4})}{1 + \frac{2}{\pi^2}|\sin(k_F)|^2} \tag{29}$$

Around $U = 0$, it is not possible to determine accurately the phase boundary between PS_1 and PS_2, due to the statistical errors in the QMC and the limited number of lattices available in the exact diagonalization studies. However, it seems clear that there will be no crossing between PS_2 phase and PS_1 phase. We believe that both phases should extend smoothly to the $U = 0$ axis and join there at the same point.

3. Numerical Results

To confirm our approximate calculations, we determined several points on the SC/PS_1 and PS_1/PS_2 phase boundaries using the QMC simulations discussed in previous section. These points were obtained by studying the behavior of correlation and response functions. In Fig. 3 we plot the transition points determined from the QMC simulations. We see that for $U > 4t$, the QMC results agree with our estimates from the strong coupling analyses to within the statistical error bars.

Our exact diagonalization studies also permit us to determine the nature of the pairing state in the regions of dominant superconducting fluctuations. From the renormalization group and g-ology studies of case $\rho = 1$ [7], we know that the dominant pairing symmetry can be different in different parameter regions; indeed, Fig. 2 shows the existence of and boundary between singlet and triplet superconducting states at 1/2 filling. Using exact diagonalization techniques, we have calculated the pairing correlation functions for on-site singlet, nearest-neighbor singlet, and nearest-neighbor triplet pairing, as defined in Section III. A typical case is shown in Fig. 6. As for $\rho = 1$, we find for *all* ρ that the dominant pairing for $U > 0$ is nearest-neighbor triplet, while for $U < 0$, the dominant pairing is on-site singlet. However, the relative strengths of the various pairings change substantially with ρ.

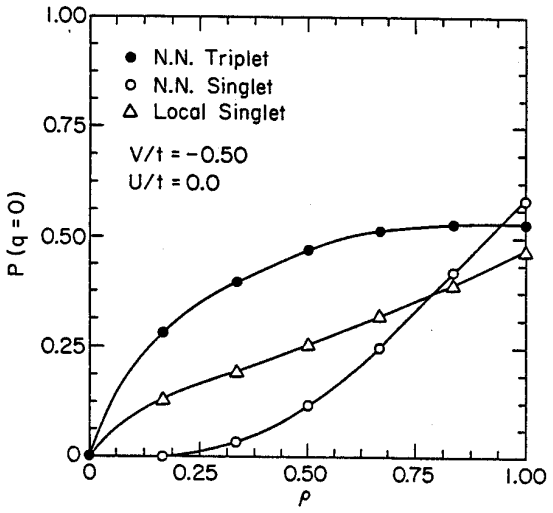

FIG. 6. Various superconducting pairing correlation functions (see text) from Lanczös exact diagonalizations versus band filling ρ for $V = -0.50t$, $U = 0$.

IV-4. $U > 0$**,** $V > 0$

The region of positive U and V is both the most directly relevant in terms of applications to real materials and, for reasons that will become clear through our discussion, the most difficult to study. Indeed, the two principal unresolved questions concerning the phase diagram – the true nature of a possible "CDW" region at large U and V for *incommensurate* ρ and of a possible superconducting region at large V and small U for $\rho = 1/2$ [18, 19] and possibly other values of ρ [20] – both involve this region. In the ensuing discussion, we will examine these and other issues using our strong coupling, QMC, and exact diagonalization methods.

As suggested by Fig. 4, for general positive U and V and small values of ρ the system is a strongly correlated metal described by the Luttinger liquid theory. We shall focus initially on values of ρ between quarter- and half-filling. A comparison of the phase diagrams depicted in Figs. 2 and 3 shows considerable differences between these two cases. We begin by recalling certain features of the familiar half-filled case.

For the half-filled case, both strong and weak coupling approaches give the phase boundary between CDW and SDW as described by equation $U = 2V$. In the intermediate coupling region, Hirsch [12] has studied CDW to SDW transition using quantum Monte Carlo simulations and found some small corrections to the $U = 2V$ phase boundary, which have been confirmed by additional numerical/analytical work [15] and higher order perturbation theory [17]. Further, as indicated in Fig. 2, the *character* of the phase "transition" changes as one goes from weak to strong coupling [12, 14, 15]. To understand how the phase diagram changes as ρ decreases from 1, we start by considering two separate strong coupling limits: (1) $V \to \infty$ and (2) $U \to \infty$.

When $V \to \infty$, configurations in the ground state will have no electrons next to each other. Spin-up and spin-down electrons can occupy the same site, but once they do they must stay together forever to avoid the infinite potential energy V. Therefore the system has in effect no spin degrees of freedom and behaves like spinless fermions. However, it still has charge degrees of freedom, and a transition to a CDW is possible.

To study this possible transition we begin with the 1/4-filled case. A perfect CDW state at $\rho = 1/2$ has (among others with similar site occupancy but different spin arrangements) the real-space configuration of electrons shown in Fig. 1(b) with energy $E = 0$. As noted previously, this specific configuration (1) corresponds to both a "$4k_F$" CDW and a $2k_F$ SDW; and (2) for $V \to \infty$, is degenerate with 2^{N_e+1} other configurations in which electrons occupy every other site but have their spins oriented differently. When V becomes finite and for $t \neq 0$, however, this specific configuration acquires lower energy from an effective attractive super-exchange interaction, and the $4k_F$ CDW and $2k_F$ SDW coexist. To study the boundary between the $\rho = 1/2$ CDW and the Luttinger liquid state, consider putting two electrons with opposite spins on top of each other; this creates a "conducting" state with the configuration shown in Fig. 7(a), where double occupied site behaves like a wall with an infinite potential (because $V \to \infty$ so that the wave function must be zero on the wall) but to the left and the right of the wall we have two free holes that move on a lattice with an open boundary. Assuming that the original lattice had N sites and the two chains separated by the doubly occupied site have, respectively, N_1 and N_2 sites, with $N = N_1 + N_2 + 1$, we have that the energy of this state is

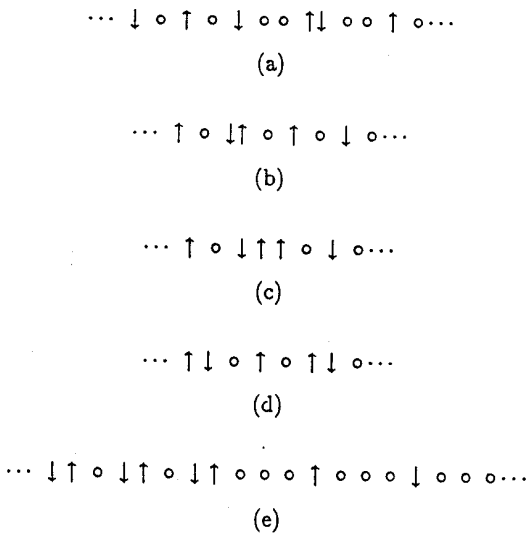

FIG. 7. Various strong coupling configurations at band fillings between quarter and half filling: (a) a excited configuration with $\rho = 1/2$ and one double occupancy; (b) a configuration contributing to the ground state at $\rho = 5/8$ for $V \gg U/2 \gg t$; (c) a configuration contributing to the ground state at $\rho = 5/8$ for $U \gg 2V \gg t$; (d) a second configuration contributing to the ground state at $\rho = 5/8$ for $U \gg 2V \gg t$; note the presence of two (soliton/domain wall) defects; (e) a potential "phase-separated" configuration for small U and $\rho = 1/2$.

$$E = U - 2t\ (\ \cos(k_1) + \cos(k_2)\ ) \tag{30}$$

where $k_{1,(2)} \simeq \frac{\pi}{N_{1,(2)}}$. The lowest energy occurs when $k_{1,2} \to 0$; this can be achieved in the thermodynamic limit: $N_{1,2} \to \infty$. At this value of $k_{1,(2)}$, we have $E = U - 4t$, so the transition to the CDW occurs at $U = 4t$.

For finite lattices, k_1 and k_2 are different from zero, and the transition from the Luttinger liquid to the CDW may occur at smaller values of U. It is straightforward to show that the critical value of U is smaller by an amount of $\frac{8\pi^2 t}{N^2}$. For example, for $N = 16$ we get $U = 3.69t$.

Apart from their utility in analyses of numerical data, such finite-size effects are important for the insight they provide into the behavior as ρ increases from 1/2 to 1. We recall that for $V \to \infty$, at half-filling the ground state is a period 2 CDW for any value of U. For $\rho > 1/2$, the $V \to \infty$ ground state *must* contain more than one doubly occupied site and hence it is divided into many small regions, bounded by the doubly occupied sites, in which the electrons are "confined". Inside these smaller regions, the individual transitions to the CDW occur at values of $U < 4t$ (as our above finite-size results show), and these values decrease as a function of ρ from $4t$ at $\rho = 1/2$ to 0 when $\rho = 1$ (*i.e.*, the configuration in Fig. 1(a) is the ground state for $V \to \infty$ for any value of U). For finite V, a second-order perturbation theory calculation yields

$$U = 4t + \frac{8t^3}{V^2}, \tag{31}$$

and we see that this line, which is shown in Fig. 3 (the dashed line labeled (a)) for the case of $\rho = 1/2$, is very steep.

We can also study the boundary between the Luttinger liquid and the CDW region in the limit $U \to \infty$, by treating the Hamiltonian as a spinless fermion model, which in turn, can be mapped into XXZ model. For $V > 2t$, the model is in the *anti*-ferromagnetic Ising region, which corresponds to the CDW state. For $V < 2t$, the model becomes XY-like, and there is no gap in excitation spectrum. Here the model belongs to the Luttinger liquid class. Hence the transition point for the CDW to TLL is at $V = 2t$. As U decreases from infinity, we expect the transition line to move to increasing V, and indeed a second-order perturbation theory calculation for finite U gives the boundary

$$V = 2t + \frac{2t^2}{U - 4t} \tag{32}$$

This line is also shown in Fig. 3(a) as the dashed line labeled (b). For $4t < U < 8t$, we used QMC simulations to determine transition point. The QMC results were not far from the curve described by Eq. (32), even for $U < 8t$. For example, QMC estimates the transition point to be $V = (3.20 \pm 0.15)t$ at $U = 6t$, while Eq. (32) gives $V = 3t$. Interpolating the QMC results and our two strong coupling curves Eqs. (31) and (32), we obtain CDW phase boundary for the case of 1/4-filled as shown in Fig. 3.

The nature of the "CDW" region for other values of ρ seems more problematic: the range of the Coulomb interactions in the extended Hubbard model leads to commensurability effects with the lattice *only* for $\rho = 1/2$, so any CDW for $\rho > 1/2$ is *incommensurate*. In ordinary

weak-coupling analyses, such incommensurate CDW's, while possibly having a single particle gap, also possess "phason" modes, which in the absence of other effects (*e.g.*, impurity trapping, disorder) lead to collective ("sliding") CDW motion and "Fröhlich" superconductivity.

To clarify this situation for intermediate and strong coupling, we perform extensive QMC simulations and establish that, for large $U(\simeq 8t)$, the CDW susceptibility exhibits a strong peak at $q = \pi$ for $V \geq U/2$ for *all* ρ greater than 1/2. This peak increases as a function of N, reflecting a transition to some sort of long-range order with spatial period 2. The boundary of the "CDW" region versus ρ for $U = 8t$ are shown in Fig. 4. As discussed above, for the large V part, the phase boundary moves towards the $U = 0$ axis as ρ approaches 1 from $1/2$. Our numerics show that for $1/2 < \rho < 1$, this boundary is *above* $U = 2V$, *i.e.*, it moves *up* from the half-filled value for $\rho < 1$.

Further insight into this "CDW" region for $\rho > 1/2$, again comes from the strong-coupling limit. We start with U, $V \gg t$ and consider separately the two cases $V \gg U/2 \gg t$ and $U \gg 2V \gg t$. For $V \gg U/2 \gg t$ and $\rho > 1/2$, the ground state will consist of an *ordered* "picket fence" of particles on every other site *plus* the appropriate number of double occupancies to reach the required electron density (see Fig. 7(b)). At $t = 0$, all orderings of the double occupancies are degenerate, so in general we expect a *disordered* array of double occupancies on the background "picket fence". Hence the charge susceptibility is expected to show a period 2 ($q = \pi$) response, with no other prominent feature. Nonetheless, the charge gap, defined as $\Delta_c(N; N_e) = E(N; N_e + 1) + E(N; N_e - 1) - 2E(N, Ne)$ is zero. Second-order perturbation theory shows that these double occupancies can move, albeit with greatly reduced hopping ($t_{eff} \simeq t^2/(2V - U)$), so that the phase in this region can best be thought of as a "heavy" Luttinger liquid (HLL), with greatly reduced conductivity.

Turning to the case $U \gg 2V \gg t$, we see that here double occupancies are essentially forbidden, and that for $\rho > 1/2$, the excess electrons beyond the "picket fence" on alternate sites must go *between* the occupied sites. This situation is illustrated in Fig. 7(c). Again we can readily find that the charge gap is 0, since the energy is (to leading order) directly proportional to the number of "interstitial" electrons, $E(N;; N(\rho - 1/2)) = 2N(\rho - 1/2)V$. In fact, as in the case of the spin 1/2 anti-ferromagnet and as indicated in Fig. 7(d), a single "interstitial" electron corresponds to *two* excitations, which can propagate independently along the chain with hopping t. Reflection on Fig. 7(d) shows that these excitations are "domain walls", or "solitons", which separate the two possible orderings (even sites or odd sites) of the $\rho = 1/2$ CDW, and which can therefore be expected to wash out this ordering away from quarter-filling. Indeed, in this region our QMC data show no peak at π away from $\rho = 1/2$. The system is behaving as a "soliton Luttinger liquid", a concept which has recently been suggested and explored in the context of infinitely repulsive, long range interactions [41].

For band filling $\rho < 1/2$, there is no CDW state, and the system is simply a Luttinger liquid. As we discussed earlier, the properties of Luttinger liquid are characterized by the exponent K_ρ. For some special cases, K_ρ can be obtained analytically. At $V = 0$, the dependence of K_ρ on the density ρ and U/t has been discussed in detail by Schulz [30]. For the quarter-filled band case at large U, the known results [42] for the XXZ model can be used to obtain:

$$K_\rho = \frac{1}{2 + (4/\pi)\sin^{-1}(V/2t)}. \tag{33}$$

Further analytic insight can be obtained by noting that the exponent $K_\rho \to 1/2$ in the limit

$\rho \to 0$ for any value of V. For $U \gg t$ and $V < V_c$, the extended Hubbard model reduces to the $t-J$ Hamiltonian with $J = t^2/(U-V)$ for which $K_\rho \to 1/2$ as $\rho \to 1$. Therefore, all contour lines $1/2 < K_\rho < 1$ should connect the two points V_c at $\rho = 1$ and $V = 0$ at $\rho = 0$. This is exactly the behavior seen in Fig. 4.

All these analytic considerations provide guidance to, and are consistent with, our numerical calculations of K_ρ, which are plotted in Fig. 4. Note that the contour lines $K_\rho = 1/2$ behave differently above and below $\rho = 1/2$. In fact, the general trend below quarter filling is similar to the spinless fermion problem, while above $\rho = 1/2$, all contour lines move toward V_c, avoiding the TLL/CDW transition boundary line at 1/4-filling. To support further the statement that outside the regions discussed above the system behaves as a TLL, we have calculated the central charge c by fitting the finite-size corrections to the ground state energy at density $\rho = 1/2$. We find $c \sim 1$ for $U = 8t, -1 < v < 2$ and for $U = 0$, $0 < v < 4$.

V. Summary and open issues

Our combined numerical and analytic investigation of the one-dimensional extended Hubbard model has revealed a phase diagram exhibiting complex structure as a function of the Coulomb interactions U and V and the band filling ρ. As shown in Figs. 2, 3, and 4, which provide the most succinct overview of our results, in much of its parameter space the model behaves as a strongly correlated metal – the "Luttinger liquid" – but there are also large regions of parameters in which various broken symmetry phases are realized. We shall organize our remaining comments around these different types of broken symmetry.

For positive U and V, *charge density wave* phases compete with the Luttinger liquid. Strong-coupling perturbation theory provides accurate semi-*quantitative* determination of the TLL/CDW boundary, which is confirmed by QMC simulations. The CDW phases exhibit strong band-filling dependence, with the true insulating states occurring only for the commensurate values of ρ corresponding to half- and quarter-filling. Nonetheless, for $1/2 < \rho < 1$ and $V \gg U/2 \gg t$, we found a "mixed" state, in which apparent long-range charge order (as shown by the divergence of $C(q = \pi)$ as $N \to \infty$) coexists with a weak conductivity mediated by the motion of disordered local pairs. A detailed understanding of this "heavy Luttinger liquid" regime is one of the interesting open problems identified by our study.

For large negative U and V, the *phase separated states* PS_1 (for $V \gg 0, U > 0$) and PS_2 (for U, $V \gg 0$) become the ground state. As indicated by Figs. 2 and 3, the boundaries of these phases show relatively weak band-filling dependence and can again be quite accurately determined by strong-coupling arguments, confirmed by QMC simulations.

From several perspectives, the occurrence of *superconducting phases* is one of the most interesting features of the extended Hubbard model. Intuitively, one expects these superconducting phases to be adjacent to the phase-separated regions because attractive interactions exist in both phases; this has been found in a number of models, in both one and two dimensions (see, *e.g.*, [40]). As shown in Figs. 2 and 3, our results confirm this expectation for the familiar "negative U" superconducting phases, both singlet and triplet. The band-filling dependence of the boundary of the superconducting phase is illustrated in Fig. 5, which quantifies the intuitive result that the boundary moves to more positive values of V for lower band fillings because it is easier for the paired electrons to "avoid" occupying neighboring sites at small ρ. Although one might anticipate that "direct" attractive interactions – *i.e.*, *negative* values of U and V – are needed

for electron pairing, previous work [40] has shown that these direct attractive interactions are not a necessary condition for superconductivity, and that it is possible to find superconductivity if there exists a mechanism, such as long-range Coulomb repulsion, that causes fluctuations in the phase-separated state. In the case of the one-dimensional extended Hubbard model, there exists another phase separated phase, as discussed by Penc and Mila [19], and by Sano and Ono [20]. This third phase separated state, PS_3, has been argued [19] to exist for large *positive* V and $|U| \simeq t$, in which one portion of the lattice consists of alternating doubly-occupied and empty sites which are frozen in place by the large positive V while the remainder of the electrons can move throughout the rest of the lattice (but avoiding occupying neighboring sites) to gain maximum kinetic energy. It was suggested that near the PS_3 phase separated region there may be such a region of superconductivity. Recently, we have studied the PS_3 phase extensively [43] and we found that the PS_3-type phase separation extends to much lower values of V than reported by other groups [19, 20]. As a result, the Luttinger liquid exponent K_ρ does not exceed one before phase separation, and hence the ground state is not dominated by superconducting fluctuations.

One further issue that remains unresolved by our study is the precise boundary of the (negative U, positive V) region in which the system behaves as a Luttinger liquid from the perspective of the charge degrees of freedom but exhibits a gap in the spin excitations (the "Luther-Emery phase"). In the absence of a careful finite-size scaling analysis, which our limited number of lattice sizes presently precludes us from undertaking, determining this phase boundary for general ρ represents an interesting open problem.

Finally, let us recall briefly some possible applications of our results to real materials. We noted in the Introduction that in contrast to the pure Hubbard model, the extended Hubbard model permits binding of particle-hole pair excitations and hence can describe excitonic effects known to be important in many novel electronic materials [1, 4]. Further, for the extended Hubbard model there is a region of parameters in which $K_\rho < 0.50$, and therefore we can expect strong diffuse X-ray scattering at $4k_F$ [44]. To make detailed comparisons with data from real materials, however, it is typically important to include electron-phonon ($e-p$) interactions as well, and one is naturally led to the class of "Peierls-extended Hubbard" models [1]. Importantly, the $(e-p)$ interactions permit the existence of additional broken symmetry states – for example, "bond order wave" (BOW) and "spin Peierls" (SP) states – which can have LRO in the ground state. The interplay among and possible coexistence of these many broken symmetries can have dramatic and varying effects, particularly in materials away from half filling [45]. The detailed explanations of the many novel phenomena observed in the quasi-one-dimensional, strongly correlated materials remains the most significant open issue, one which will form the basis of many further investigations.

Acknowledgments

We owe a great deal to our beloved colleague, Dr. E. R. Gagliano, who unfortunately passed away before the completion of this article. We thank W. Somsky and J. E. Gubernatis for their collaboration on the initial quantum Monte Carlo calculations, V. J. Emery for many useful discussions and valuable comments. It is also a pleasure to thank many colleagues for conversations related to this subject, including S. Bacci, J. Carmelo, M. P. A. Fisher, G. Gomez-Santos, H. E. Hirsch, S. Mazumdar, K. Penc, M. Randeria, H. J. Schulz, P. van Dongen, and J. Voit. Part of this work were done during HQL's visit to National Taiwan University (NTU) and he is very grateful to colleagues at Physics Department of NTU for their support and friendship.

Partial support for HQL by the Research Grants Council of Hong Kong SAR and for DKC by NSF grant DMR-8920538 is gratefully acknowledged. Most of computations were performed at the National Center for Supercomputing Applications, University of Illinois at Urbana-Champaign, the National Energy Research Supercomputer Center, Lawrence Livermore National Laboratory, and Los Alamos National Laboratory. We are grateful for their support.

References

[1] For an overview, written in the specific context of conducting polymers, that presents a discussion of the broader context of electron-electron (and electron-phonon) interactions in novel electronic materials in reduced dimensions, see D. Baeriswyl, D. K. Campbell, and S. Mazumdar pp. 7-134 in *Conjugated Conducting Polymers*, H. Kiess, ed. (Springer, Berlin, 1992).

[2] D. Poilblanc *et al*., Europhys. Lett. **22**, 537 (1993).

[3] E. H. Lieb and F. Y. Wu, Phys. Rev. Lett. **20**, 1445 (1968).

[4] Dandan Guo *et al*., Phys. Rev. B **48**, 1433 (1993).

[5] W. P. Su and J. R. Schrieffer, Phys. Rev. Lett. **46**, 735 (1981).

[6] S. Mazumdar, H. Q. Lin, and D. K. Campbell, in *Organic Superconductivity* eds., V. Z. Kresin and W. A. Little (Plenum, 1990) pp. 221-229, and references therein.

[7] V. J. Emery, in *Highly Conducting One-Dimensional Solids*, eds. by J. T. Devreese *et al.* (Plenum, New York, 1979) pp. 247-303.

[8] J. Solyom, Adv. in Physics **28**, 201 (1979).

[9] B. Fourcade and G. Sproken, Phys. Rev. B **29**, 5089 (1984).

[10] A. Luther and I. Peschel, Phys. Rev. B **9**, 2911 (1974); D. C. Mattis, J. Math. Phys. **15**, 609 (1974); J. Cannon and E. Fradkin, Phys. Rev. B **41**, 9435 (1990); J. Voit, Phys. Rev. B **45**, 4027 (1992).

[11] L. Milas del Bosch and L. M. Falicov, Phys. Rev. B **37**, 6073 (1988); B. Fourcade and G. Sproken, Phys. Rev. B **29**, 5096 (1984).

[12] J. E. Hirsch, Phys. Rev. Lett. **53**, 2327 (1984).

[13] J. E. Hirsch and D. J. Scalapino, Phys. Rev. B **27**, 7169 (1983); **29**, 5554 (1984).

[14] H. Q. Lin and J. E. Hirsch, Phys. Rev. B **33**, 8155 (1986).

[15] J. Cannon, R. Scallettar, and E. Fradkin, Phys. Rev. B **44**, 5995 (1991).

[16] V. J. Emery, Phys. Rev. B **14**, 2989 (1976); see also M. Fowler, Phys. Rev. B. **17**, 2989 (1978); K. B. Efetov and A. I. Larkin, Sov. Phys. JETP, **42**, 390 (1976).

[17] See P. J. van Dongen, to be published in *The Hubbard Model: Proceedings of the 1993 NATO ARW on "The Physics and Mathematical Physics of the Hubbard Model"*, eds., D. Baeriswyl *et al.* (Plenum, 1995).

[18] F. Mila and X. Zotos, Europhys. Lett. **24**, 133 (1993).

[19] K. Penc and F. Mila, Phys. Rev. B **49**, 9670 (1994).

[20] K. Sano and Y. Ono have recently published exact diagonalization studies of small systems for $\rho = 1/2$ and $\rho = 2/3$, determining K_ρ by assuming the validity of the Luttinger liquid relations. See K. Sano and Y. Ono, J. Phys. Soc. Japan **63**, 1250 (1994).

[21] F. D. M. Haldane, Phys. Rev. Lett. **45**, 1358 (1980); F. D. M. Haldane, J. Phys. C **14**, 2585 (1981).

[22] H. Q. Lin *et al*., to be published in *The Hubbard Model: Proceedings of the 1993 NATO ARW on "The Physics and Mathematical Physics of the Hubbard Model"*, eds., D. Baeriswyl *et al.* (Plenum, 1995).

[23] E. Lieb and D. C. Mattis, J. Math. Phys. **6** 304 (1965).

[24] S. Coleman, Phys. Rev. D **11**, 2088 (1975).

[25] S. Mandelstam, Phys. Rev. D **11**, 3026 (1975).
[26] J. E. Hirsch *et al*., Phys. Rev. B. **26**, 5033 (1982).
[27] H. Q. Lin and J. E. Gubernatis, Comput. Phys. **7**, 400 (1993); see also E. R. Gagliano *et al.*, Phys. Rev. B **34**, 1677 (1986).
[28] S. Tomonaga, Prog. Theor. Phys. **5**, 544 (1950); J. M. Luttinger, J. Math. Phys. **4**, 1154 (1963).
[29] For a history of many-body problems in one dimension from a perspective especially relevant for this article, see V. J. Emery, in *Correlated Electron Systems*, ed. V. J. Emery, (World Scientific, 1993) pp. 166-198, and references therein.
[30] H. J. Schulz, Phys. Rev. Lett. **64**, 2831 (1990); H. J. Schulz, Int. J. Mod. Phys. B **5**, 57 (1991).
[31] H. Frahm and V. E. Korepin, Phys. Rev. B **42**, 10553 (1990); Phys. Rev. B **43**, 5643 (1991).
[32] N. Kawakami and S. K. Yang, Phys. Rev. Lett. **65**, 2309 (1990); Phys. Lett. A **148**, 359 (1990); J. M. P. Carmelo, P. Horsch and A. A. Ovchinnikov, Phys. Rev. B **46**, 14728 (1992).
[33] C. A. Stafford, A. J. Millis, and B. S. Shastry, Phys. Rev. B **43**, 13660 (1991).
[34] R. M. Fye *et al*., Phys. Rev. B **44**, 6909 (1991).
[35] E. Gagliano and C. Balseiro, *Phys. Rev. Lett.* **59**, 2999 (1987).
[36] M. Ogata *et al*., Phys. Rev. Lett. **66**, 2388 (1991); F. F. Assaad and D. Würtz, Phys. Rev. B **44**, 2681 (1991).
[37] For a comprehensive review, see R. Micnas, J. Ranninger, S. Robaszkiewicz, Rev. Mod. Phys. **62**, 113 (1990).
[38] D. J. Klein and W. A. Seitz, Phys. Rev. B **10**, 3217 (1974).
[39] H. Bethe, Zeits f. Physik **71**, 205 (1931).
[40] S. A. Kivelson, V. J. Emery, and H. Q. Lin, Phys. Rev. B **42**, 6523 (1990).
[41] G. Gomez-Santos, Phys. Rev. Lett. **70**, 3780 (1993).
[42] A. Luther and I. Peschel, *Phys. Rev. B* **12**, 3908 (1975).
[43] R. T. Clay, A. W. Sandvik, and D. K. Campbell, Phys. Rev. B **59**, 4665 (1999).
[44] Many quasi-one-dimensional compounds show this $4k_F$ feature in diffuse X-ray scattering. For more details see, J.P. Pouget, in *Highly Conducting Quasi-One-Dimensional Crystal Semiconductors and Semimetals* (Pergamon, New York, 1988) p. 87.
[45] S. Mazumdar, D. Toussaint, and K.-C. Ung, Phys. Rev. Lett. **73**, 2603 (1994).